Check for updates

Impact of non-thermal variables on hydroxylated GDGT distributions around Iceland

David J. Harning[1]* and Julio Sepúlveda[1,2]

[1]Institute of Arctic and Alpine Research, University of Colorado, Boulder, CO, United States,
[2]Department of Geological Sciences, University of Colorado, Boulder, CO, United States

Archaeal isoprenoid glycerol dibiphytanyl glycerol tetraethers (GDGTs) preserved in sediments are popular tools for the reconstruction of past temperature in the global ocean. Whereas the most common GDGTs have been well studied through environmental and culture studies, their hydroxylated version (OH-GDGTs) is just emerging as a new proxy. Some empirical evidence suggests that the distribution of OH-GDGTs may capture sea surface temperature variability. However, the effects of additional environmental factors on OH-GDGT distributions have not been rigorously tested, and evidence suggests that salinity, sea ice, seasonality, terrestrial input, and water depth may be additional factors in some settings. In this study, we analyzed the distribution of OH-GDGTs in modern and Holocene marine sediment from the North Iceland Shelf. By statistically comparing the biomarker datasets against a collection of modern instrumental and paleoceanographic records, we separated which environmental variables may be controlling OH-GDGT-derived proxies around Iceland. In contrast to prevailing theory, we found that nitrate concentrations and water-column stratification are best correlated to OH-GDGT distributions, and not temperature. These results hold important implications for the application of OH-GDGT proxies in high-latitude oceans, particularly in highly stratified locations, as well as for future studies on the biological sources and functionality of these lipids. Given the current complexity of proxy interpretation, we urge caution in the current application of OH-GDGTs as a tool in paleotemperature reconstructions.

KEYWORDS

Iceland, marine sediment, proxy, lipid biomarkers, GDGTs

1 Introduction

Marine ammonia oxidizing Thaumarchaeota (Marine Group 1.1a, recently reclassified to Nitrososphaerota; Rinke et al., 2021) are among the most widespread and abundant organisms in the ocean, accounting for up to 40% of microbial plankton (Karner et al., 2001; Francis et al., 2005; Könneke et al., 2005). Thaumarchaeota play a central role in the nitrogen cycle by performing the first and rate-limiting step of nitrification, i.e., the oxidation of ammonium (NH_4^+) or ammonia (NH_3) to nitrite (NO_2^-) (Könneke et al., 2005; Beman et al., 2008; Newell et al., 2013), and are therefore most abundant near or below the photic zone (Francis et al., 2005; Church et al., 2010). The predominant membrane spanning lipids of Thaumarchaeota are isoprenoid glycerol dibiphytanyl glycerol tetraethers (GDGTs), which contain 0 to 4 cyclopentane rings (GDGT-0 to GDGT-4) as well as an

additional GDGT than contains four cyclopentane rings and one cyclohexane ring (crenarchaeol) (Sinninghe Damsté et al., 2002; Schouten et al., 2013). Culture experiments of various Thaumarchaeota taxa show that the degree of cyclization is controlled by ambient temperature through a process known as homeoviscous adaptation (Wuchter et al., 2004; Elling et al., 2015), although other factors such as growth phase (Elling et al., 2014), oxygen availability (Qin et al., 2015), and ammonnia oxidation rates (Hurley et al., 2016) can also influence GDGT distributions. The degree of cyclization, expressed through various iterations of the TEX_{86} index (i.e., tetraether index of tetraethers consisting of 86 carbons), has therefore been exploited as a temperature proxy across a range of geologic periods and geographical settings (e.g., Schouten et al., 2002; Schouten et al., 2013).

While widely applied, the uncertainty in global GDGT-temperature calibrations increases at both the cool and warm ends of the temperature spectrum (Schouten et al., 2002; Kim et al., 2010). Regional and spatially varying calibrations that can capture the nuances of local oceanographic regimes have been able to reduce this uncertainty for some locations (Shevenell et al., 2011; Tierney and Tingley, 2014; Harning et al., 2019; Harning et al., 2023). For polar regions, it has also been noted that a related class of Thaumarchaeota lipids, i.e., hydroxylated GDGTs (OH-GDGTs, Lipp and Hinrichs, 2009; Liu et al., 2012a; Elling et al., 2017; Bale et al., 2019), increase in fractional abundance relative to low latitude regions (Huguet et al., 2013; Varma et al., 2024a). As the addition of one hydroxyl group may further reduce membrane rigidity at lower temperatures (Huguet et al., 2017), the development of OH-GDGT-based indices that rely on the relationship between temperature and cyclization (0–2 cyclopentane rings) have been proposed (e.g., RI-OH and RI-OH', Lü et al., 2015), and may offer improvements upon TEX_{86}-based temperature proxies at high latitudes (Fietz et al., 2013; Huguet et al., 2013; Varma et al., 2024a). However, the effects of additional environmental factors on OH-GDGT cyclization have not been rigorously tested with cultures, and empirical evidence suggests that salinity, sea ice, seasonality, terrestrial input, and water depth may be complicating factors in some settings (Fietz et al., 2013; Kang et al., 2017; Lü et al., 2019; Park et al., 2019; Wei et al., 2020; Sinninghe Damsté et al., 2022; Harning et al., 2023; Xiao et al., 2023; Varma et al., 2024b).

The North Iceland Shelf is one of the most studied regions in North Atlantic Holocene paleoceanography and hosts a diversity of proxy records for temperature, salinity, and nutrient availability (e.g., Kristjánsdóttir et al., 2017). In addition to a network of modern surface sediments that support many of the local downcore proxy interpretations (e.g., Helgadóttir, 1997), these records provide important opportunities to cross-validate each another and better inform the functionality of individual proxies. In this study, we take advantage of modern surface sediments and Holocene sediment records previously analyzed for isoprenoid GDGTs (Harning et al., 2019) and present new corresponding data for OH-GDGTs. To better understand which environmental factor(s) may drive OH-GDGT distributions on Iceland's insular shelves, we statistically compare modern surface sediment samples with instrumental datasets as well as Holocene sediments with independent proxy records that capture physical-chemical parameters. Collectively, our analyses demonstrate that OH-GDGT distributions around Iceland may be influenced by nutrient availability and water column

stratification, and that caution should be exercised when applying OH-GDGT-derived indices to reconstruct past temperature in some high-latitude regions.

2 Methods

2.1 Marine sediment samples

We investigated marine surface sediments ($n = 11$) and Holocene sediment cores ($n = 2$) from Iceland's insular shelves that have previously been analyzed for isoprenoid GDGTs (Harning et al., 2019). Marine surface sediments were collected in July 1997 during the cooperative United States/Icelandic *Bjarni Sæmundsson* (B997) research cruise (Helgadóttir, 1997) and span a gradient of oceanographic conditions around Iceland today (Figure 1) and range from 112 to 658 m below sea level (mbsl) (Harning et al., 2019). Holocene sediment core MD99-2269 (66.63 °N, 20.85 °W; 365 mbsl) is located on the western North Iceland Shelf and under the primary influence of the North Iceland Irminger Current (NIIC, Atlantic Water) whereas core JR51-GC35 (67.33 °N, 16.70 °W; 420 mbsl) lies on the eastern North Iceland Shelf and is mainly influenced by the East Iceland Current (EIC, Arctic Water, Figure 1). MD99-2269 features a robust Holocene age model derived from 27 AMS ^{14}C dates, marker tephra layers (volcanic ash), and paleomagnetic secular variation (Kristjánsdóttir et al., 2007; Stoner et al., 2007), of which 20 AMS ^{14}C dates cover the last 8,000 years. JR51-GC35's age model is based on 10 ^{14}C dates, of which eight span the last 8,000 years (Bendle and Rosell-Melé, 2007). Given that sedimentation rates are nearly linear at both locations over the last 8,000 years, we do not present proxy records as mass accumulation rates.

2.2 Archaeal hydroxylated GDGTs (OH-GDGTs)

We extracted and analyzed all samples as detailed in Harning et al. (2019). Briefly, we extracted B997 surface sediments three times on a Dionex accelerated solvent extractor (ASE 200) using dichloromethane:methanol (9:1, v/v) at 100°C and 2,000 psi (Harning et al., 2019), whereas samples from MD99-2269 ($n = 53$) and JR51-GC35 ($n = 18$) sediments were extracted via ultrasonication using dichloromethane:methanol (2:1, v/v) (Harning et al., 2021). We then dissolved a 50% TLE aliquot of each sample in hexane:isopropanol (99:1, v/v), followed by filtration using a 0.45 μm polytetrafluoroethylene (PTFE) syringe. Prior to instrumental analysis, we spiked samples with 10 ng of the C46 GDGT internal standard (Huguet et al., 2006). We identified and quantified OH-GDGTs on a Thermo Scientific Ultimate 3,000 HPLC system interfaced to a Q Exactive Focus Orbitrap-Quadrupole MS (Harning et al., 2019) using modified methods of Hopmans et al. (2016) and characteristic mass spectra and retention times (Liu et al., 2012a; Liu et al., 2012b).

We explore two OH-GDGT temperature indices developed for relatively warmer and cooler regions, respectively (Lü et al., 2015):

$$RI - OH = \frac{[OH - GDGT - 1] + 2x[OH - GDGT - 2]}{[OH - GDGT - 1] + [OH - GDGT - 2]},$$
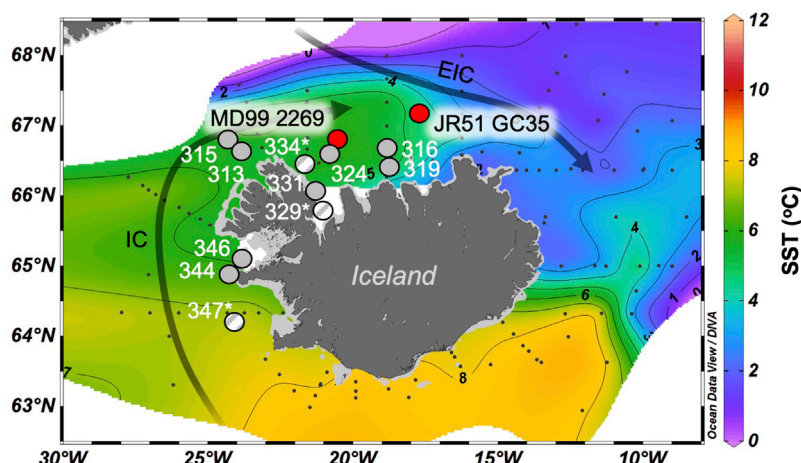
FIGURE 1
Overview map of Iceland and its insular shelves. The locations of B997 marine surface sediments are shown with gray circles, where hatched line circles and site names with asterisks denote samples without all OH-GDGTs present. The locations of the two Holocene marine sediment core records (MD99-2269 and JR51-GC35) are shown with red circles. The main ocean currents are the Irminger Current (IC, Atlantic Water) and the East Icelandic Current (EIC, Arctic Water). Base map from Ocean Data View software (Schlitzer, 2021) and displays ocean temperatures (°C) at 50 mbsl from May 2014.

$$RI-OH' = \frac{[OH-GDGT-1]+2x[OH-GDGT-2]}{[OH-GDGT-0]+[OH-GDGT-1]+[OH-GDGT-2]},$$

and convert to temperature using the following global calibrations after Varma et al. (2024a):

$$RI-OH = 0.018\,x\,SST + 1.12\,(n=744, \text{error not reported})$$

$$RI-OH' = 0.040\,x\,SST + 0.003\,(n=759, \text{error not reported})$$

We note that OH-GDGT indices are adaptations of the Ring Index, which reflects the weighted average of cyclopentane moieties in isoprenoid GDGTs (Zhang et al., 2016).

We also explore two temperature indices that combine GDGT and OH-GDGT distributions (Fietz et al., 2016; Varma et al., 2024a):

$$OH^C = \frac{[GDGT-2]+[GDGT-3]+[cren']-[OH-GDGT-0]}{[GDGT-1]+[GDGT-2]+[GDGT-3]+[cren']+[OH-GDGT-0]}$$
$$+[OH-GDGT-1]+[OH-GDGT-2],$$

$$TEX_{86}^{OH} = \frac{[GDGT-2]+[GDGT-3]+[cren']}{[GDGT-1]+[GDGT-2]+[GDGT-3]+[cren']+[OH-GDGT-0]},$$

and convert to temperature using the following global calibrations after Varma et al. (2024a):

$$OH^C = 0.043\,x\,SST - 0.53\,(n=555, \text{error not reported})$$

$$TEX_{86}^{OH} = 0.021\,x\,SST + 0.08\,(n=599, \text{error not reported})$$

2.3 Statistical analyses

To explore environmental factors that may influence Icelandic OH-GDGT distributions, we statistically compared %OH, RI-OH,

RI-OH', OH^C, and TEX_{86}^{OH} sedimentary values against modern instrumental data as well as sediment proxy datasets. For the modern surface sediment samples, we used instrumental World Ocean Atlas 2018 (WOA18) decadal mean datasets from 1995 to 2004 CE. Specifically, we compared OH-GDGT distributions against annual and seasonal depth integrations (every 10 m between 0 and 100 mbsl and every 25 m between 100 and 200 mbsl) for the following annual variables: temperature (Locarnini et al., 2018), salinity (Zweng et al., 2018), dissolved oxygen concentration (Garcia et al., 2018a), and nitrate concentration (Garcia et al., 2018b) (Figure 2). WOA18 temperature and salinity are provided at ¼-degree pixels and oxygen and nitrate concentrations at 1-degree pixels. We also calculated a water column stratification index based on the difference between 10 m water depth temperature and that of every depth below down to 200 m water depth (Locarnini et al., 2018). We assessed correlation significance using t-tests, where we define significance as p-values <0.05. For the Holocene sediment records, we compared OH-GDGT distributions from MD99-2269 with published proxy datasets from the same sediment core ($n = 17$, Table 1; Supplementary Figure S1). All datasets were first collapsed to the lowest common resolution leaving 47 data points per time series with an average resolution of 167 years over the last 8,000 years. Each time series was then normalized according to their mean and standard deviations. Finally, we performed hierarchal clustering using the 'stats' package in the open-source environment R (R Core Team, 2022).

3 Results

3.1 Modern surface sediments

We found OH-GDGTs in all 11 marine surface sediments, but only eight samples contain all three common OH-GDGTs (OH-GDGT-0, −1, and −2) above the detection limit required to calculate associated indices (Figure 1, gray circles). Correlations of
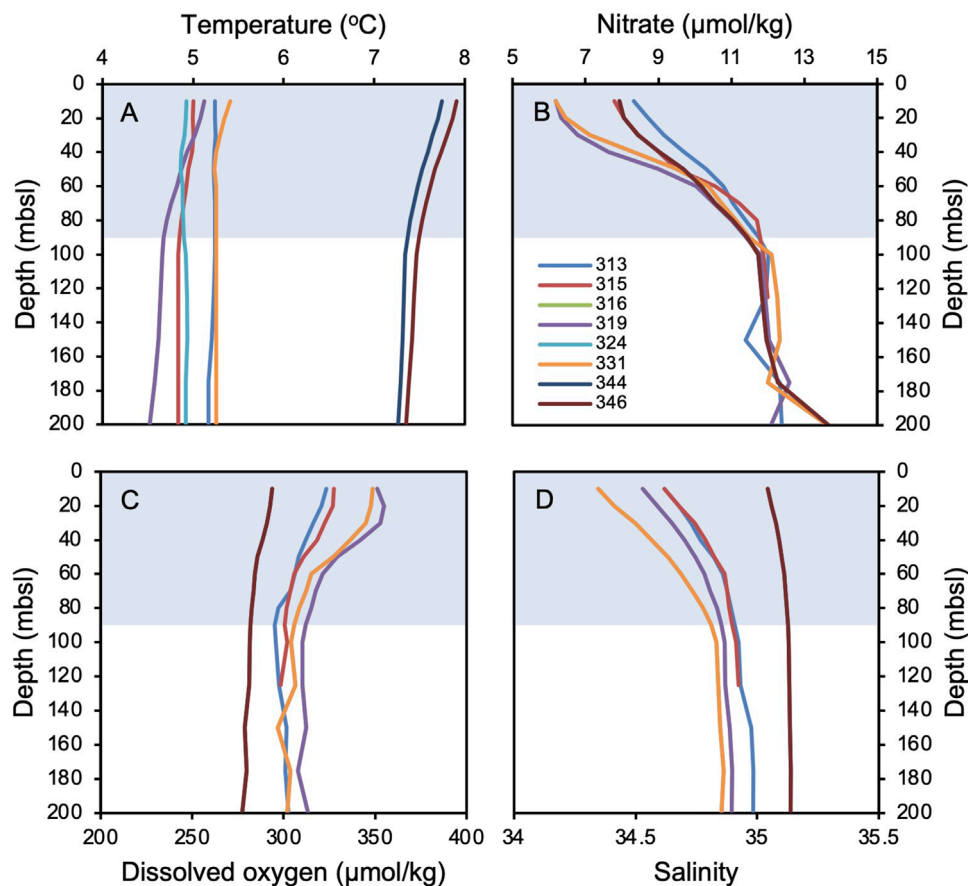
FIGURE 2
World Ocean Atlas 2018 (WOA18) mean annual decadal (1995–2004) data for each surface sediment site where all OH-GDGTs are present (see Figure 1). **(A)** temperature (Locarnini et al., 2018), **(B)** salinity (Zweng et al., 2018), **(C)** dissolved oxygen concentration (Garcia et al., 2018a), and **(D)** nitrate concentration (Garcia et al., 2018b) against depth in meters below sea level (mbsl). The blue bars highlight the deepest extent of the annual mixed layer in the water column down to ~90 mbsl, which is characterized by vertical gradients in all four variables averaged across the seasons.

sedimentary OH-GDGT indices with annual WOA18 instrumental data show that the RI-OH index has moderate correlations with nitrate concentration (max correlation at 50 mbsl, R^2 = 0.56, Figures 3B, 4A) and temperature stratification (max correlation at 80 mbsl, R^2 = 0.54, Figures 3E, 4B), and weak to no correlations with temperature (Figure 3A), dissolved oxygen (Figure 3C), and salinity (Figure 3D). The RI-OH' index shows moderate correlations with temperature (max correlation at 200 mbsl, R^2 = 0.45, Figure 3A), nitrate (max correlation at 30 mbsl, R^2 = 0.48, Figure 3B), dissolved oxygen (max correlation at 150 mbsl, R^2 = 0.64, Figure 3C), and salinity (max correlation at 175 mbsl, R^2 = 0.43, Figure 3D), but not temperature stratification (Figure 3E). The OH^C index shows moderate correlations with temperature (max correlation at 200 mbsl, R^2 = 0.42, Figure 3A) and dissolved oxygen (max correlation at 200 mbsl, R^2 = 0.45, Figure 3C), and weak correlations with nitrate (max correlation at 200 mbsl, R^2 = 0.28, Figure 3B), salinity (max correlation at 90 mbsl, R^2 = 0.38, Figure 3D), and temperature stratification (Figure 3E). The TEX$_{86}$^{OH} index is like the OH^C index but with generally weaker correlations. TEX$_{86}$^{OH} shows weak correlations with temperature (max correlation at 10 mbsl, R^2 = 0.37, Figure 3A), nitrate (max

correlation at 200 mbsl, R^2 = 0.30, Figure 3B), dissolved oxygen (max correlation at 200 mbsl, R^2 = 0.39, Figure 3C), salinity (max correlation at 90 mbsl, R^2 = 0.33, Figure 3D), and temperature stratification (Figure 3E).

Seasonal integrations of WOA18 instrumental data (i.e., winter, spring, summer, and fall) generally show similar correlations to GDGT and OH-GDGT indices as the annual WOA18 instrumental data does (Supplementary Figures S2–S5). While R^2 values vary to some degree between seasons, the relative correlations trends between environmental data and temperature, dissolved oxygen, and salinity are similar between seasons, with TEX$_{86}$^{L} typically featuring the highest R^2 values and RI-OH the lowest R^2 values (Supplementary Figures S2–S5). On the other hand, correlations between seasonal nitrate and temperature stratification and biomarker indices differ to a greater degree between seasons (Supplementary Figures S2–S5). These seasonal differences are most notable for the RI-OH index, whereas TEX$_{86}$^{L}, %OH, RI-OH', OH^C, and TEX$_{86}$^{OH} tend to feature similar correlation patterns with seasonal nitrate and temperature stratification data. For RI-OH and nitrate concentrations, correlations are weak in winter (R^2 < 0.26, Supplementary Figures S2B), moderate in spring (R^2

TABLE 1 Summary of the 17 proxy records from core MD99-2269 used in hierarchal cluster analysis and their typically inferred environmental driver(s).

Proxy	Environmental driver(s)	References
Diatom SST	Summer SST	Justwan et al. (2008)
Foraminifera SST	Annual SST	Harning et al. (2021)
TEX_{86}^L	Annual subT	Harning et al. (2021)
C. neoteretis	Atlantic bottom water	Harning et al. (2021)
C. reniforme	Arctic bottom water	Harning et al. (2021)
I. norcrossi	Arctic bottom water	Harning et al. (2021)
N. pachyderma	Arctic surface water	Harning et al. (2021)
N. labradorica	Arctic Front productivity	Harning et al. (2021)
T. quinqueloba	Arctic Front productivity	Harning et al. (2021)
IP_{25}	Seasonal sea ice	Cabedo-Sanz et al. (2016)
HBI III	Arctic Front productivity	Cabedo-Sanz et al. (2016); Harning et al. (2021)
N. pachyderma δ18O	SST and salinity	Kristjánsdóttir et al. (2017)
$C_{37:4}$	Salinity	Kristjánsdóttir et al. (2017)
$U_{37}^{K'}$	Summer SST	Kristjánsdóttir et al. (2017)
Quartz wt%	Sea ice	Moros et al. (2006)
Calcite wt%	Nutrients, SST	Moros et al. (2006)
Coccolithophores	Nutrients, SST	Giraudeau et al. (2004)

See Supplementary Figure S1 for individual proxy timeseries.

< 0.36, Supplementary Figures S3B), moderate in summer (R^2 < 0.37, Supplementary Figures S4B), and moderately strong in fall (R^2 < 0.63, Supplementary Figures S5B). For RI-OH and temperature stratification, correlations are weak in winter (R^2 < 0.25, Supplementary Figures S2E), moderate in spring (R^2 < 0.33, Supplementary Figures S3E), moderate in summer (R^2 < 0.39, Supplementary Figures S4E), and moderately strong in fall (R^2 < 0.65, Supplementary Figures S5E).

3.2 Holocene sediment records

We found all three common OH-GDGTs (OH-GDGT-0, -1, and -2) above the detection limit in sediment samples from the two Holocene records. While sampling resolution is higher for MD99-2269 (n = 53) compared to JR51-GC35 (n = 18), both records show comparable trends for RI-OH, RIOH', OH^C, and TEX_{86}^{OH} proxies at the millennial scale but with slightly lower inferred temperatures in JR51-GC35 (Figure 5). In the higher resolution MD99-2269, centennial scale variability is noisy with incremental samples often reflecting changes on the order of 1°C in all four indices (Figure 5). Similar trends and variability are also observed for %OH, which is the percent abundance of OH-GDGTs to

total GDGT and OH-GDGTs (Huguet et al., 2013), however, we do note that both records have similar %OH ranges (Figure 5). For the RI-OH index, reconstructed SSTs generally increase before reaching a maximum between ~3,200 and 2,400 BP, after which inferred SSTs decline towards present (Figure 5). For the RI-OH', OH^C, and TEX_{86}^{OH} indices, the two records show a pattern of slightly increasing SSTs towards present, with two millennial scale peaks between ~6,500 and 4,100 BP and ~2,700 and 700 BP (Figure 5). Hierarchal clustering analysis shows that the RI-OH index clusters with % calcite and coccolithophore concentrations (purple, Figure 6A) and that the RI-OH', OH^C, and TEX_{86}^{OH} indices cluster separately (orange, Figure 6A). The %OH clusters with Polar foraminifera *Nitrosopumilus pachyderma* δ18O, and do a lesser degree, alkenone related proxies C37:4 and $U_K'37$ (gray, Figure 6A). Importantly, another cluster with no OH-GDGT indices is characterized by established local temperature proxies derived from TEX_{86}^L and diatom and foraminifera assemblage transfer functions, as well as two foraminifera species (*C. reniforme* and *Nitrosopumilus quinqueloba*) related to Arctic Water masses and fronts (red, Figure 6A). Similarly, sea ice and polar related proxies (i.e., quartz, IP_{25}, and *N. pachyderma* foraminifera), which are inherently related to temperature through the advection of Polar Water masses, also cluster together (blue, Figure 6A).
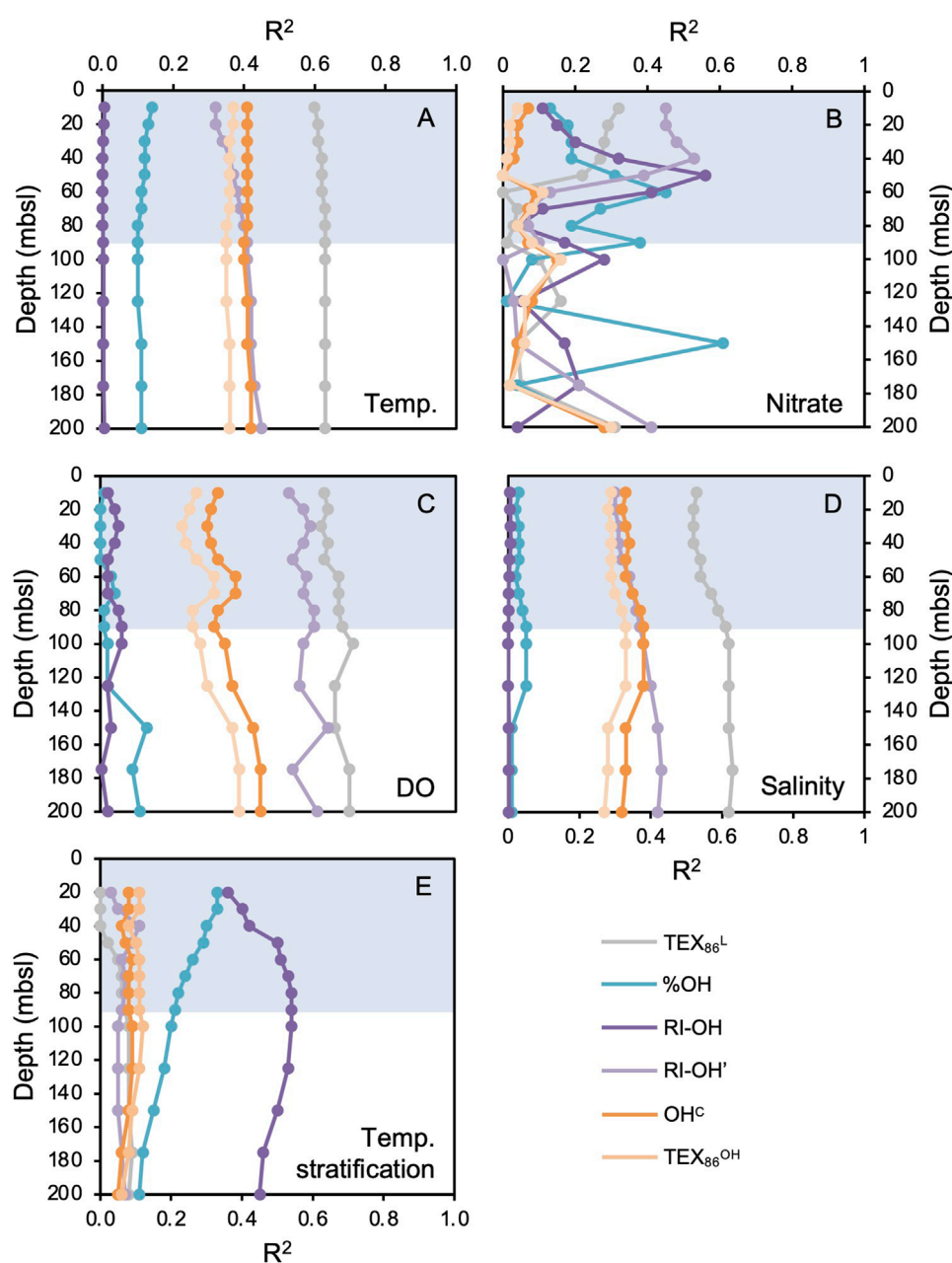
FIGURE 3
Correlations (shown as the R^2 value vs. depth) between modern surface sediment sample GDGT and OH-GDGT indices and annual WOA18 instrumental datasets for **(A)** temperature, **(B)** nitrate concentration, **(C)** dissolved oxygen concentration (DO), **(D)** salinity, and **(E)** temperature stratification, at various water depths (mbsl). For **(E)**, temperature stratification is calculated as the difference between 10 m and the depth (mbsl) indicated by the data point. The blue bars highlight the deepest extent of the annual mixed layer present in the water column down to ~90 mbsl (see Figure 2).

4 Discussion

4.1 Influence of non-thermal environmental variables on OH-GDGT distributions

4.1.1 Modern surface sediments

Along with a broader geographic network of sites (Rodrigo-Gámiz et al., 2015), surface sediment samples from Iceland's insular shelf exhibit a strong positive relationship between TEX_{86}^L

and winter subsurface temperatures (subT, Harning et al., 2019). However, OH-GDGT indices from the same region do not show comparable temperature correlations. For example, the RI-OH index's best correlations are with annual nitrate concentrations at 50 mbsl ($R^2 = 0.56$) and fall temperature stratification between 10 and 60 mbsl ($R^2 = 0.65$), both within the deepest extent of the annual mixed layer that occupies the upper 90 m of the water column (Figure 3). Correlations between RI-OH and nitrate concentrations are similarly strong in the fall compared to annual, whereas correlations between RI-OH and nitrate and
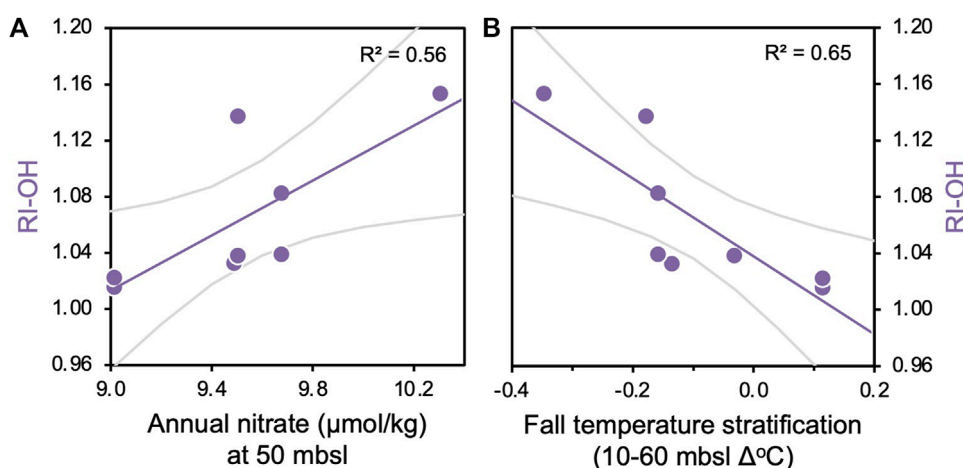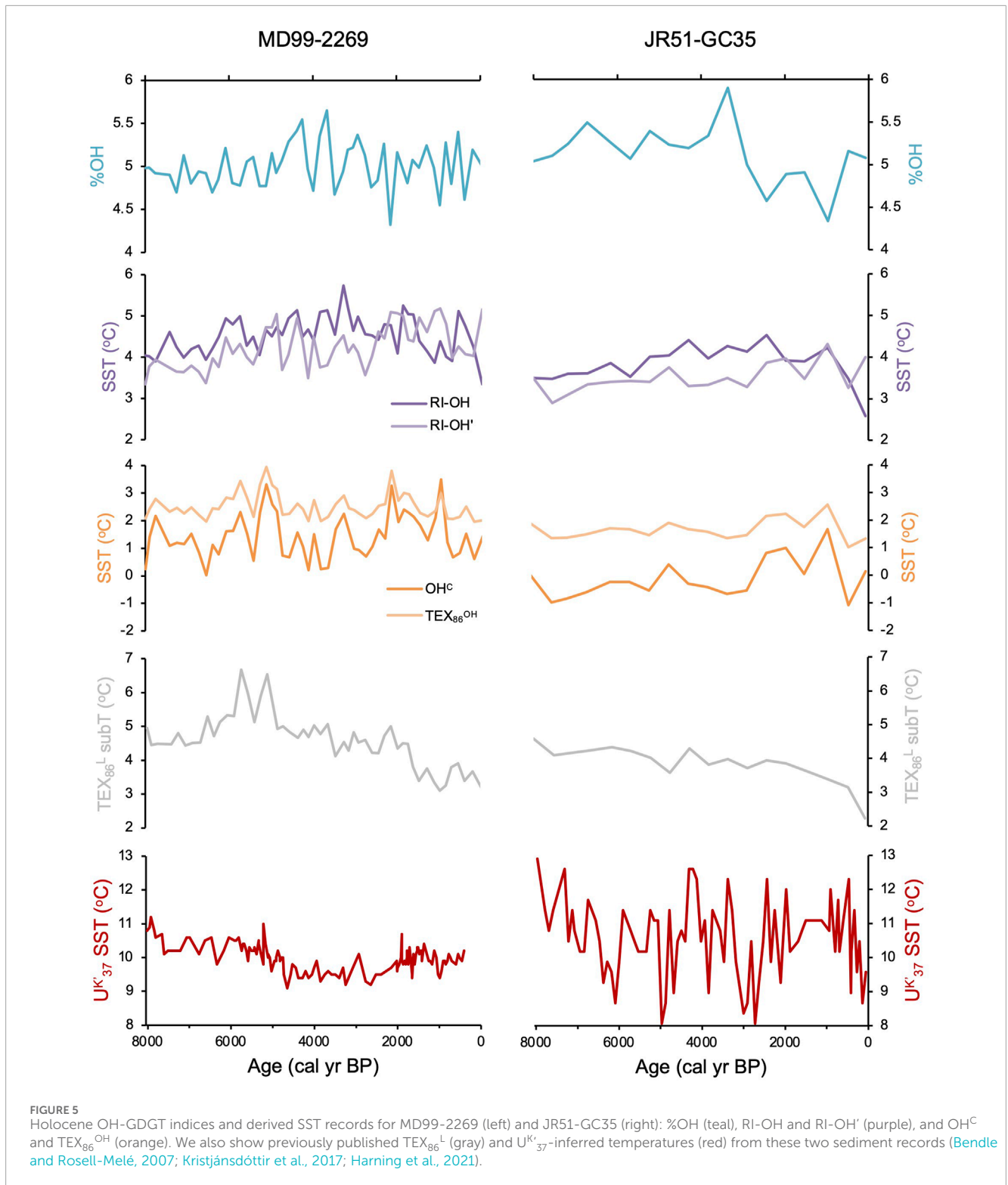
FIGURE 4
Correlations between modern surface sediment RI-OH values and **(A)** annual nitrate (μmol/kg) at 50 mbsl and **(B)** fall temperature stratification (Δ°C) between 10 and 60 m water depth. *p*-values for all regressions are <0.05.

temperature stratification are comparatively weak in the other seasons (Supplementary Figures S2–S5). This suggests a primarily fall signal for the RI-OH index. The RI-OH', OH^C, and TEX_{86}^{OH} indices then show generally weak correlations to temperature, nitrate, dissolved oxygen, and salinity (Figure 3). An exeption is that correlations between RI-OH' and annual nitrate are moderately strong at 40 mbsl, which is similar to RI-OH and annual nitrate correlation at 50 mbsl (Figure 3B). Seasonally, the RI-OH' has relatively strong correlations with fall temperature stratification in the mixed layer compared to other seasons whereas OH^C and TEX_{86}^{OH} consistently have weak correlations to all oceanographic variables compared to other biomarker indices (Supplementary Figures S2–S5). For Thaumarchaeota, the main product of their ammonia-oxidation is nitrite (Könneke et al., 2005; Beman et al., 2008; Newell et al., 2013), which can then be subsequently oxidized by bacteria to nitrate (Kuyper et al., 2018). While there is no information on nitrite from Iceland's insular shelves, we can only assume that nitrate concentrations provide indirect evidence for both reactions and that nitrate concentrations can serve as a proxy for local nitrite production. While this assumption is subjected to large uncertainty, the correlations observed with nitrate suggest that nutrient availability may exert some control on OH-GDGT distributions around Iceland.

On Iceland's insular shelves, salinity, dissolved oxygen and nutrients (i.e., nitrate, phosphate, and silica) tend to co-vary with temperature as these variables are primarily influenced by source waters (Stefánsson, 1968; Stefánsson and Ólafsson, 1991). Broadly, Atlantic Water (IC, Figure 1) dominates the west coast and is warm and saline with higher dissolved oxygen and nutrient concentrations. In contrast, on the North Iceland Shelf, Arctic Water (EIC, Figure 1), which is cool, low salinity and has lower dissolved oxygen and nutrient concentrations, underlies surface Atlantic Water (Stefánsson, 1962). This geographically variable oceanography contributes to regional stratification differences that have a strong impact on local primary
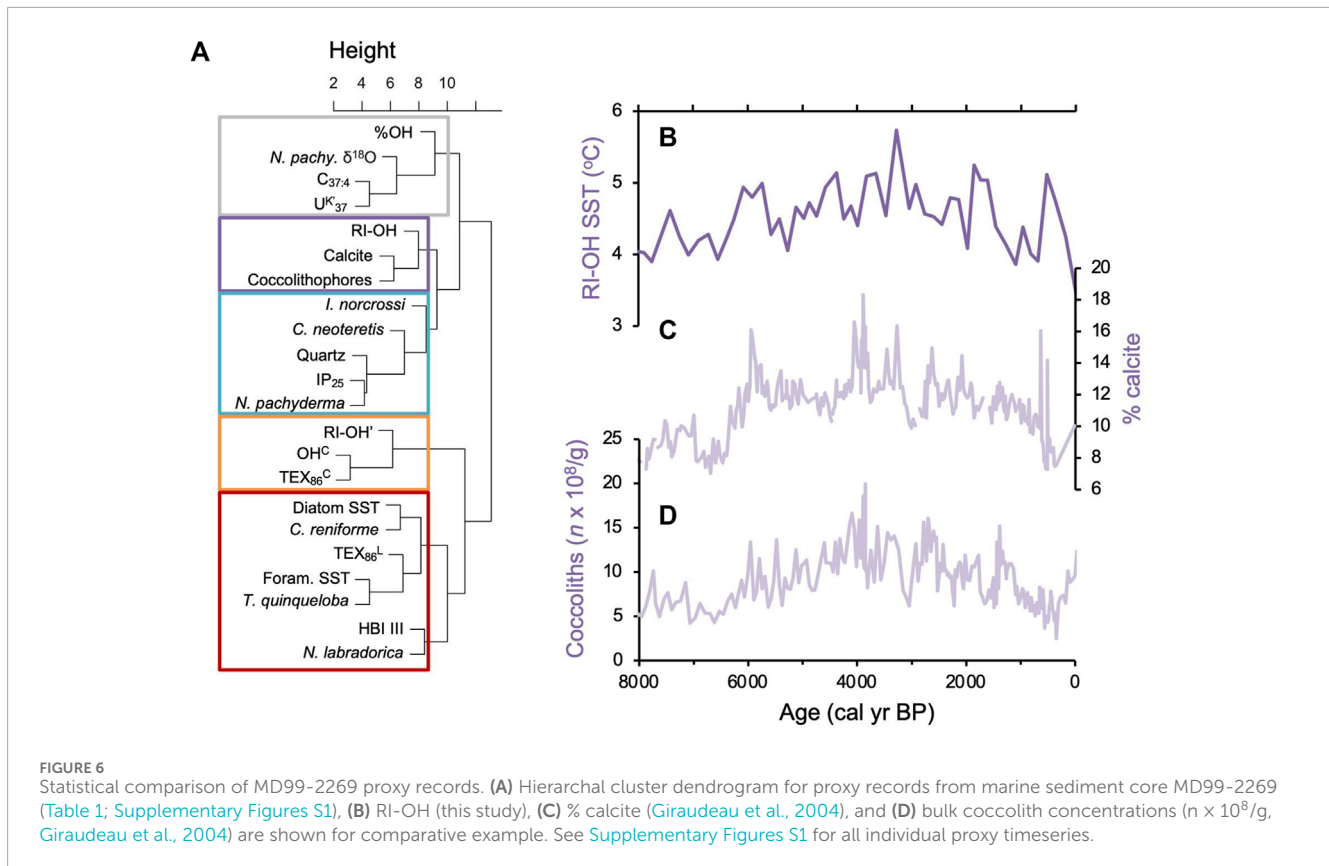
productivity (Thórdardóttir, 1984; Gudmundsson, 1998). On the North Iceland Shelf, the earlier seasonal stratification and stabilization of the water column generally results in an earlier and shorter phytoplankton bloom compared to the western shelf where series of blooms occur throughout the spring in less stratified waters (Gudmundsson, 1998). As a first-order interpretation, we may therefore expect that the shorter spring phytoplankton blooms on the North Iceland Shelf would result in less competition for Thaumarchaeota and ammonium compared to the western shelf, as Thaumarchaeota are more dominant when phytoplankton productivity is low (e.g., Pitcher et al., 2011). While we cannot definitively link our GDGT results to phytoplankton blooms, empirical evidence from water column measurements south of Iceland demonstrates that ammonia-oxidation rates increase below the euphotic zone (below 50 m water depth) in more stratified waters compared to less stratified waters (Painter, 2011).

Culture experiments of Thaumarchaeota (*Nitrosopumilus maritimus*) demonstrate that increased ammonia oxidation rates (and nitrite production) result in reduced GDGT cyclization (Hurley et al., 2016). The modern surface sediments from Iceland show that samples collected from below more stratified waters on the North Iceland Shelf have lower RI-OH values, particularly in fall (Figure 4B), which could potentially indicate that the increased ammonia-oxidation rates in such settings may also lead to reduced OH-GDGT cyclization. Under these periods of increased ammonia oxidation, we would also expect that Thaumarchaeota and bacteria would produce more nitrite and nitrate through nitrification, and therefore a negative correlation would exist between RI-OH and nitrate concentrations. However, we observe a positive correlation between OH-GDGT cyclization and nitrate (Figure 4A). In contrast to our expectations, Painter (2011) observe lower concentrations of nitrate under the more stratified Icelandic waters that lead to increased ammonia oxidation rates. While the mechanisms behind the relationship between ammonia oxidations rates and nitrate concentrations are currently unclear, the correlations

FIGURE 5
Holocene OH-GDGT indices and derived SST records for MD99-2269 (left) and JR51-GC35 (right): %OH (teal), RI-OH and RI-OH' (purple), and OH^C and TEX$_{86}$OH (orange). We also show previously published TEX$_{86}$^{L} (gray) and U$^{K'}_{37}$-inferred temperatures (red) from these two sediment records (Bendle and Rosell-Melé, 2007; Kristjánsdóttir et al., 2017; Harning et al., 2021).

observed between nitrate, water column stratification and RI-OH values (Figure 4) are consistent with local observations of water column stratification and nitrogen cycling (Painter, 2011) as well as culture experiments of Thaumarchaeota response to ammonia oxidation rates (Hurley et al., 2016). Future research

on the relative roles of bacteria and archaea in local nitrification will be instrumental to clarify these observations and contribute to our knowledge of the North Atlantic's nitrogen cycle which so far has largely focused on nitrogen fixation [see review by Benavides and Voss (2015)].

FIGURE 6
Statistical comparison of MD99-2269 proxy records. **(A)** Hierarchal cluster dendrogram for proxy records from marine sediment core MD99-2269 (Table 1; Supplementary Figures S1), **(B)** RI-OH (this study), **(C)** % calcite (Giraudeau et al., 2004), and **(D)** bulk coccolith concentrations (n × 10^8/g, Giraudeau et al., 2004) are shown for comparative example. See Supplementary Figures S1 for all individual proxy timeseries.

4.1.2 Holocene sediments

Hierarchal cluster analysis shows that the RI-OH-inferred SSTs form a cluster with coccolithophore productivity proxies around Iceland (Figure 6A i.e., coccolith concentrations and biogenic calcite; Andrews and Giraudeau, 2003). Along with additional proxy records from the same sediment core, the coccolith and calcite records from MD99-2269 (Giraudeau et al., 2004) have previously been interpreted to reflect water column stratification and nutrient availability over the North Iceland Shelf, where the Early (11,700–8,200 BP) and Late Holocene (4,200 BP to present) were more stratified and nutrient limited than the Middle Holocene (8,200–4,200 BP, Kristjánsdóttir et al., 2017; Harning et al., 2021). Early Holocene water column stratification was likely due to freshwater contributions from residual northern hemisphere ice sheet melt (e.g., Jennings et al., 2015), and during the Late Holocene, due to freshwater and Polar water associated with the increased export of sea ice through Fram Strait (Müller et al., 2012; Cabedo-Sanz et al., 2016). Like the modern surface sediments, we observe a negative relationship between RI-OH-inferred SSTs and proxies reflecting stratification (Figures 6B–D). Following Section 4.1.1, we hypothesize that the Early and Late Holocene periods of increased stratification could have resulted in increased Thaumarchaeota productivity, possibly increased ammonia-oxidation rates, and thus reduced cyclization of OH-GDGTs (lower RI-OH, Figure 6B). The reduced productivity of haptophyte algae at these times (Figures 6C,D) would also reduce competition for ammonia with Thaumarchaeota, which may have further contributed to increased ammonia-oxidation rates (lower RI-OH) (Smith et al., 2014).

Hierarchal cluster analysis shows that the RI-OH', OH^C, and TEX$_{86}$^{OH} indices are unrelated to other established temperature proxies from the region (Figure 6A), including GDGT-based TEX$_{86}$^{L} (Harning et al., 2019) and diatom and foraminifera assemblage transfer functions (Justwan et al., 2008; Harning et al., 2021). This is supported by the modern surface sediment samples that generally show weak to moderate correlations between these indices and temperature as well as the other tested environmental variables (i.e., nitrate, dissolved oxygen, and salinity, Figure 3; Supplementary Figures S2–S5). The %OH, which has been suggested to reflect temperature in some marine settings (Huguet et al., 2013; Varma et al., 2024a), clusters most closely with *N. pachyderma* δ^{18}O, and then to a slightly less extent, alkenone related indices C$_{37:4}$ and U$^{K'}_{37}$ (Figure 6A). *N. pachyderma* δ^{18}O and the relative abundance of C$_{37:4}$ have been interpreted to capture local changes in salinity on Holocene timescales (Kristjánsdóttir et al., 2017), and recent evidence from the Canadian Arctic shows that increased abundance of C$_{37:4}$ is linked to a sea-ice associated lineage of haptophyte (Isochrysidales) distinct from other known alkenone-producing (e.g., *Emiliania huxleyi* and *Gephyrocapsa oceanica*) (Wang et al., 2021). Regarding the latter, increased contributions of C$_{37:4}$ during the Late Holocene (Kristjánsdóttir et al., 2017) likely reflect changes in the local haptophyte community that may have therefore impacted the U$^{K'}_{37}$ index, which is typically used a temperature proxy (e.g., Brassell et al., 1986). This may be one reason why U$^{K'}_{37}$ clusters separately from other temperature proxies, i.e., TEX$_{86}$^{L} and diatom and foraminifera assemblage transfer functions (Figure 6A). In any case, the clusters for RI-OH', OH^C,

and TEX_{86}^{OH} and %OH add further evidence that temperature is not the most significant control of OH-GDGT distributions through the Holocene.

Quantitative climate histories derived from other Icelandic paleoceanographic (e.g., Ólafsdóttir et al., 2010; Jiang et al., 2015; Moossen et al., 2015) and terrestrial records (e.g., Harning et al., 2020) agree that local Holocene climate was characterized by first order cooling due to declining Northern Hemisphere summer insolation. Within the marine realm, these first order changes in Holocene climate led to changes in water column stratification and nutrient availability (Giraudeau et al., 2004; Kristjánsdóttir et al., 2017), as well as more complex changes in ocean biogeochemistry related to the migration of the Arctic and Polar marine fronts during the Middle and Late Holocene (Harning et al., 2021). Yet, despite the well characterized oceanographic conditions of the North Iceland Shelf during the Holocene, the changes in the RI-OH', OH^C, and TEX_{86}^{OH} indices are challenging to reconcile for a couple reasons. First, their relative patterns generally show increasing temperatures over the last 8,000 years (Figure 5), which is inconsistent with northern hemisphere summer insolation, the primary modulator of North Atlantic climate on millennial timescales (Moros et al., 2004; Jiang et al., 2015; Kristjánsdóttir et al., 2017). Second, the two broad peaks in temperature identified between ~6,500 and 4,100 BP and ~2,700 and 700 BP (Figure 5) occur under contrasting oceanographic regimes on the North Iceland Shelf. The former period between ~6,500 and 4,100 BP is characterized by a proximal Arctic Front that enhanced pelagic productivity, while the latter period between ~2,700 and 700 BP was characterized by the presence of sea-ice-bearing Arctic and Polar Water that displaced the Arctic Front southward resulting in decreased local pelagic productivity due to nutrient limitation (Harning et al., 2021). Therefore, while currently unclear, we conclude that due to the incompatibility with other paleoceanographic and terrestrial climate proxies around Iceland, the RI-OH', OH^C, and TEX_{86}^{OH} proxies do not likely reflect SST on the North Iceland Shelf as shown for the current global dataset, including cooler polar regions (Varma et al., 2024a).

4.2 Possible implications for biological source and physiological adaption

Lipidomic studies of thaumarchaeal cultures demonstrate that all core GDGTs and OH-GDGTs measured in this study can be derived from Thaumarchaeota Group 1.1a (Elling et al., 2017; Bale et al., 2019). However, additional archaeal groups have also been found to produce GDGTs and OH-GDGTs, including the closely related ammonia-oxidizing SAGMCG-1 (Elling et al., 2017), a methanogen *Methanococcus thermolithotrophicus* (Liu et al., 2012), and an anaerobic methanotroph ANME-2d (Kurth et al., 2019). Given that the distributions of GDGTs and OH-GDGTs around Iceland correlate with different environmental factors (i.e., marine temperature and stratification, respectively), it is possible that the different lipid classes derive from different microbial producers including but not limited to those currently known. Recent evidence using intact polar lipids and 16S rRNA from the Baltic Sea suggests that in some marine regions, *Nitrosopumilus*, one dominant taxa within the

Thaumarchaeota Group 1.1a phylum, may differ physiologically from representative taxa in other regions (Wittenborn et al., 2023). In addition, intact polar lipid and genomic studies also show that the broader GDGT lipidome varies between epipelagic and deep water-dwelling archaea (Francis et al., 2005; Hallam et al., 2006; Hu et al., 2011; Villanueva et al., 2014), where each zone has its own thermal regulation of GDGTs and OH-GDGTs (Zhu et al., 2016). Without the added insight from polar headgroup distributions (e.g., Zhu et al., 2016), it is not currently possible to attribute Icelandic GDGT and OH-GDGT distributions to different archaea depth habitats.

If the biological producer is the same for both lipid classes around Iceland, such as Thaumarchaeota Group 1.1a from one depth habitat, our data suggest that the addition of a hydroxyl group may alternatively be advantageous for non-thermal stressors related to stratification and nutrient availability. As microbial studies on Iceland's shelves are currently limited to ^{13}C-labeling of sedimentary Thaumarchaeota (Lengger et al., 2014) and baseline microbial assemblage inventories (Jégousse et al., 2021; 2022), the reasons for the differences we currently observe between GDGTs and OH-GDGTs are largely speculative. Future work combining lipidomics (including both core and intact polar lipids) and genomics, as well as culture experiments that isolate potential drivers, will be required to yield process-based insight into the functionality of OH-GDGTs in archaeal lipid membranes and test if varying archaeal lineages may contribute to their local distribution (e.g., Villanueva and Coolen, 2022).

5 Conclusion

The application of OH-GDGTs in high-latitude paleoclimate reconstructions is in a relative state of infancy (Knies et al., 2014; Kremer et al., 2018; Allaart et al., 2020) despite their widespread abundance in marine settings (Varma et al., 2024a). This may be in part due to general uncertainties regarding their functionality in archaeal cell membranes and response to environmental stressors (e.g., Fietz et al., 2020). Around Iceland, a wealth of modern and paleoceanographic data derived from marine sediment exist to empirically test the control of environmental variables on local OH-GDGT distributions. In this study, we compared OH-GDGT distributions in a network of modern surface sediments with modern oceanographic data, and in two Holocene marine sediment records with published paleoceanography records. We found that unlike temperature dependent GDGT-based indices, nitrate concentrations and thermal water-column stratification are best correlated to OH-GDGT distributions. These results hold important implications for the application of OH-GDGTs as paleotemperature proxies in high-latitude oceans particularly in regions that experience water column stratification. Specifically, the data suggest that caution should be exercised when using OH-GDGTs as temperature indicators in some regions until further culturing and calibrating work is conducted. In addition, the data motivate future work on OH-GDGTs as a proxy for stratification and nitrogen availability.

Data availability statement

The raw data supporting the conclusions of this article will be made available by the authors, without undue reservation.

Author contributions

Funding

Acknowledgments

Conflict of interest

The authors declare that the research was conducted in the absence of any commercial or financial relationships that could be construed as a potential conflict of interest.

Publisher's note

All claims expressed in this article are solely those of the authors and do not necessarily represent those of their affiliated organizations, or those of the publisher, the editors and the reviewers. Any product that may be evaluated in this article, or claim that may be made by its manufacturer, is not guaranteed or endorsed by the publisher.

Supplementary material

The Supplementary Material for this article can be found online at: https://www.frontiersin.org/articles/10.3389/feart.2024.1430441/full#supplementary-material

References

Allaart, L., Müller, J., Schomacker, A., Rydningen, T. A., Håkansson, L., Kjellman, S. E., et al. (2020). Late Quaternary glacier and sea-ice history of northern Wijdefjorden, Svalbard. *Boreas* 49, 417–437. doi:10.1111/bor.12435

Andrews, J. T., and Giraudeau, J. (2003). Multi-proxy records showing significant Holocene environmental variability: the inner N. Iceland Shelf (Húnaflói). *Quat. Sci. Rev.* 22, 175–193. doi:10.1016/s0277-3791(02)00035-5

Bale, N. J., Palatinszky, M., Rijpstra, W. I. C., Herbold, C. W., Wagner, M., and Sinninghe Damsté, J. S. (2019). Membrane lipid composition of the moderately thermophilic ammonia-oxidizing archaeon "*Candidatus Nitrosotenuis uzonensis*" at different growth temperatures. *Appl. Environ. Microbiol.* 85, 013322–e1419. doi:10.1128/aem.01332-19

Beman, J. M., Popp, B. N., and Francis, C. A. (2008). Molecular and biogeochemical evidence for ammonia oxidation by marine Crenarchaeota in the Gulf of California. *ISME J.* 2, 429–441. doi:10.1038/ismej.2007.118

Benavides, M., and Voss, M. (2015). Five decades of N_2 fixation research in the North Atlantic ocean. *Front. Mar. Sci.* 2. doi:10.3389/fmars.2015.00040

Bendle, J. A. P., and Rosell-Melé, A. (2007). High-resolution alkenone sea surface temperature variability on the North Icelandic Shelf: implications for Nordic Seas palaeoclimatic development during the Holocene. *Holocene* 17, 9–24. doi:10.1177/0959683607073269

Brassell, S. C., Eglinton, G., Marlowe, I. T., Pflaumann, U., and Sarnthein, M. (1986). Molecular stratigraphy: a new tool for climatic assessment. *Nature* 320, 129–133. doi:10.1038/320129a0

Cabedo-Sanz, P., Belt, S. T., Jennings, A. E., Andrews, J. T., and Geirsdóttir, Á. (2016). Variability in drift ice export from the Arctic Ocean to the North Icelandic Shelf over the last 8000 years: a multi-proxy evaluation. *Quat. Sci. Rev.* 146, 99–115. doi:10.1016/j.quascirev.2016.06.012

Church, M. J., Wai, B., Karl, D. M., and DeLong, E. F. (2010). Abundances of crenarchaeal amoA genes and transcripts in the Pacific Ocean. *Environ. Microbiol.* 12, 679–688. doi:10.1111/j.1462-2920.2009.02108.x

Elling, F. J., Könneke, M., Lipp, J. S., Becker, K. W., Gagen, E. J., and Hinrichs, K. U. (2014). Effects of growth phase on the membrane lipid composition of the thaumarchaeon Nitrosopumilus maritimus and their implications for archaeal lipid distributions in the marine environment. *Geochim. Cosmochim. Acta* 141, 579–597. doi:10.1016/j.gca.2014.07.005

Elling, F. J., Konneke, M., Mubmann, M., Greve, A., and Hinrichs, K. U. (2015). Influence of temperature, pH, and salinity on membrane lipid composition and TEX_{86} of marine planktonic thaumarchaeal isolates. *Geochim. Cosmochim. Acta* 171, 238–255. doi:10.1016/j.gca.2015.09.004

Elling, F. J., Könneke, M., Nicol, G. W., Stieglmeier, M., Bayer, B., Spieck, E., et al. (2017). Chemotaxonomic characterisation of the thaumarchaeal lipidome. *Environ. Microbiol.* 19, 2681–2700. doi:10.1111/1462-2920.13759

Fietz, S., Ho, S. L., and Huguet, C. (2020). Archaeal membrane lipid-based paleothermometry for applications in polar oceans. *Oceanography* 33. doi:10.5670/oceanog.2020.207

Fietz, S., Ho, S. L., Huguet, C., Rosell-Melé, A., and Martínez-García, A. (2016). Appraising GDGT-based seawater temperature indices in the Southern Ocean. *Org. Geochem.* 102, 93–105. doi:10.1016/j.orggeochem.2016.10.003

Fietz, S., Huguet, C., Rueda, G., Hambach, B., and Rosell-Melé, A. (2013). Hydroxylated isoprenoidal GDGTs in the nordic seas. *Mar. Chem.* 152, 1–10. doi:10.1016/j.marchem.2013.02.007

Francis, C. A., Roberts, K. J., Beman, J. M., Santoro, A. E., and Oakley, B. B. (2005). Ubiquity and diversity of ammonia-oxidizing archaea in water columns and sediments of the ocean. *Proc. Natl. Acad. Sci.* 102, 14683–14688. doi:10.1073/pnas.0506625102

Garcia, H. E., Weathers, K., Paver, C. R., Smolyar, I., Boyer, T. P., Locarnini, R. A., et al. (2018a). *World Ocean Atlas 2018, volume 3: dissolved oxygen, apparent oxygen utilization, and oxygen saturation*. Editor A. Mishonov Technical (NOAA Atlas NESDIS), 83, 38.

Garcia, H. E., Weathers, K., Paver, C. R., Smolyar, I., Boyer, T. P., Locarnini, R. A., et al. (2018b). in *World Ocean Atlas 2018, volume 4: dissolved inorganic nutrients (phosphate, nitrate and nitrate+nitrite, silicate)*. Editor A. Mishonov Technical (NOAA Atlas NESDIS 84), 35.

Giraudeau, J., Jennings, A. E., and Andrews, J. T. (2004). Timing and mechanisms of surface and intermediate water circulation changes in the Nordic Seas over the last 10,000 cal years: a view from the North Iceland Shelf. *Quat. Sci. Rev.* 23, 2127–2139. doi:10.1016/j.quascirev.2004.08.011

Gudmundsson, K. (1998). Long-term variation in phytoplankton productivity during spring in Icelandic waters. *ICES J. Mar. Sci.* 55, 635–643. doi:10.1006/jmsc.1998.0391

Hallam, S. J., Mincer, T. J., Schleper, C., Preston, C. M., Roberts, K., Richardson, P. M., et al. (2006). Pathways of carbon assimilation and ammonia oxidation suggested by environmental genomic analyses of marine Crenarchaeota. *PLoS. Biol.* 4, e95–e536. doi:10.1371/journal.pbio.0040095

Harning, D. J., Andrews, J. T., Belt, S. T., Cabedo-Sanz, P., Geirsdóttir, Á., Dildar, N., et al. (2019). Sea ice control on winter subsurface temperatures of the North Iceland Shelf during the Little Ice Age: a TEX$_{86}$ calibration case study. *Paleoceanogr. Paleoclimatol.* 34, 1006–1021. doi:10.1029/2018pa003523

Harning, D. J., Curtin, L., Geirsdóttir, Á., D'Andrea, W. J., Miller, G. H., and Sepúlveda, J. (2020). Lipid biomarkers quantify Holocene summer temperature and ice cap sensitivity in Icelandic lakes. *Geophys. Res. Lett.* 47, e2019GL085728. doi:10.1029/2019gl085728

Harning, D. J., Holman, B., Woelders, L., Jennings, A. E., and Sepúlveda, J. (2023). Biomarker characterization of the North water polynya, baffin bay: implications for local sea ice and temperature proxies. *Biogeosciences* 20, 229–249. doi:10.5194/bg-20-229-2023

Harning, D. J., Jennings, A. E., Köseoğlu, D., Belt, S. T., Geirsdóttir, Á., and Sepúlveda, J. (2021). Response of biological productivity to North Atlantic marine front migration during the Holocene. *Clim. Past.* 17, 379–396. doi:10.5194/cp-17-379-2021

Helgadóttir, G. (1997). *Paleoclimate (0 to >14 ka) of W and NW Iceland: an Iceland/USA contribution to P.A.L.E. Cruise report B9-97 R/V Bjarni Sæmundsson RE 30 17th–30th july 1997.* (Reykjavík, Iceland: Marine Research Institute of Iceland).

Hopmans, E. C., Schouten, S., and Sinninghe Damsté, J. S. (2016). The effect of improved chromatography on GDGT-based palaeoproxies. *Org. Geochem.* 93, 1–6. doi:10.1016/j.orggeochem.2015.12.006

Hu, A. Y., Jiao, N. Z., and Zhang, C. L. L. (2011). Community structure and function of planktonic crenarchaeota: changes with depth in the South China Sea. *Microb. Ecol.* 62, 549–563. doi:10.1007/s00248-011-9866-z

Huguet, C., Fietz, S., and Rosell-Melé, A. (2013). Global distribution patterns of hydroxy glycerol dialkyl glycerol tetraethers. *Org. Geochem.* 57, 107–118. doi:10.1016/j.orggeochem.2013.01.010

Huguet, C., Fietz, S., Rosell-Melé, A., Daura, X., and Costenaro, L. (2017). Molecular dynamics simulation study of the effect of glycerol dialkyl glycerol tetraether hydroxylation on membrane thermostability. *Biochim. Biophys. Acta Biomembr.* 1859, 966–974. doi:10.1016/j.bbamem.2017.02.009

Huguet, C., Hopmans, E. C., Febo-Ayala, W., Thompson, D. H., Sinninghe Damsté, J. S., and Schouten, S. (2006). An improved method to determine the absolute abundance of glycerol dibiphytanyl glycerol tetraether lipids. *Org. Geochem.* 37, 1036–1041. doi:10.1016/j.orggeochem.2006.05.008

Hurley, S. J., Elling, F. J., Könneke, M., Buchwald, C., Wankel, S. D., Santoro, A. E., et al. (2016). Influence of ammonia oxidation rate on thaumarchaeal lipid composition and the TEX$_{86}$ temperature proxy. *Proc. Natl. Acad. Sci.* 113, 7762–7767. doi:10.1073/pnas.1518534113

Jégousse, C., Vannier, P., Groben, R., Glöckner, F. O., and Marteinsson, V. T. (2021). A total of 219 metagenome-assembled genomes of microorganisms from Icelandic marine waters. *PeerJ* 9, e11112. doi:10.7717/peerj.11112

Jégousse, C., Vannier, P., Groben, R., Guðmundsson, K., and Marteinsson, V. T. (2022). Marine microbial communities of north and south shelves of Iceland. *Front. Mar. Sci.* 9, 1–13. doi:10.3389/fmars.2022.795835

Jennings, A. E., and Andrews, J. T., and Wilson, L. (2015). Detrital carbonate events on the Labrador shelf, a 13 to 7 kyr template for freshwater forcing from the Laurentide Ice Sheet. *Quat. Sci. Rev.* 107, 62–80. doi:10.1016/j.quascirev.2014.10.022

Jiang, H., Muscheler, R., Björck, S., Seidenkrantz, M.-S., Olsen, J., Sha, L., et al. (2015). Solar forcing of Holocene summer sea-surface temperatures in the northern North Atlantic. *Geology* 43, 203–206. doi:10.1130/g36377.1

Justwan, A., Koc, N., and Jennings, A. E. (2008). Evolution of the Irminger and East Icelandic Current systems through the Holocene, revealed by diatom-based sea surface temperature reconstructions. *Quat. Sci. Rev.* 27 (15-16), 1571–1582. doi:10.1016/j.quascirev.2008.05.006

Kang, S., Shin, K. H., and Kim, J. H. (2017). Occurrence and distribution of hydroxylated isoprenoid glycerol dialkyl glycerol tetraethers (OH-GDGTs) in the Han River system, South Korea. *Acta Geochim.* 36, 367–369. doi:10.1007/s11631-017-0165-3

Karner, M. B., DeLong, E. F., and Karl, D. M. (2001). Archaeal dominance in the mesopelagic zone of the Pacific Ocean. *Nature* 409, 507–510. doi:10.1038/35054051

Kim, J.-H., van der Meer, J., Schouten, S., Helmke, P., Willmott, V., Sangiorgi, F., et al. (2010). New indices and calibrations derived from the distribution of crenarchaeal isoprenoid tetraether lipids: Implications for past sea surface temperature reconstructions. *Geochimica et Cosmochimica Acta* 74 (16), 4639–4654. doi:10.1016/j.gca.2010.05.027

Knies, J., Cabedo-Sanz, P., Belt, S. T., Baranwa, S., Fietz, S., and Rosell-Melé, A. (2014). The emergence of modern sea ice cover in the Arctic Ocean. *Nat. Comm.* 5, 5608. doi:10.1038/ncomms6608

Könneke, M., Bernhard, A. E., de la Torre, J. R., Walker, C. B., Waterbury, J. B., and Stahl, D. A. (2005). Isolation of an autotrophic ammonia-oxidizing marine archaeon. *Nature* 437, 543–546. doi:10.1038/nature03911

Kremer, A., Stein, R., Fahl, K., Ji, Z., Yang, Z., Wiers, S., et al. (2018). Changes in sea ice cover and ice sheet extent at the Yermak Plateau during the last 160 ka: reconstructions from biomarker records. *Quat. Sci. Rev.* 182, 93–108. doi:10.1016/j.quascirev.2017.12.016

Kristjánsdóttir, G. B., Moros, M., Andrews, J. T., and Jennings, A. E. (2017). Holocene Mg/Ca, alkenones, and light stable isotope measurements on the outer North Iceland shelf (MD99-2269): a comparison with other multi-proxy data and sub-division of the Holocene. *Holocene* 26, 55–62. doi:10.1177/0959683616652703

Kristjánsdóttir, G. B., Stoner, J. S., Jennings, A. E., Andrews, J. T., and Grönvold, K. (2007). Geochemistry of Holocene cryptotephras from the North Iceland Shelf (MD99-2269): intercalibration with radiocarbon and palaeomagnetic chronostratigraphies. *Holocene* 17, 155–176. doi:10.1177/0959683607075829

Kurth, J. M., Smit, N. T., Berger, S., Schouten, S., Jetten, M. S. M., and Welte, C. U. (2019). Anaerobic methanotrophic archaea of the ANME-2d clade feature lipid composition that differs from other ANME archaea. *FEMS Microbiol. Ecol.* 95, fiz082. doi:10.1093/femsec/fiz082

Kuypers, M. M. M., Marchant, H. K., and Kartal, B. (2018). The microbial nitrogen-cycling network. *Nat. Rev. Microbiol.* 16, 263–276. doi:10.1038/nrmicro.2018.9

Lengger, S. K., Lipsewers, Y. A., de Haas, D., Sinninghe-Damsté, J. S., and Schouten, S. (2014). Lack of ^{13}C-label incorporation suggests low turnover rates of thaumarchaeal intact polar tetraether lipids in sediments from the Iceland shelf. *Biogeosciences* 11, 201–216. doi:10.5194/bg-11-201-2014

Lipp, J. S., and Hinrichs, K.-U. (2009). Structural diversity and fate of intact polar lipids in marine sediments. *Geochim. Cosmochim. Acta* 73, 6816–6833. doi:10.1016/j.gca.2009.08.003

Liu, X.-L., Lipp, J. S., Simpson, J. H., Lin, Y.-S., Summons, R. E., and Hinrichs, K.-U. (2012a). Mono- and dihydroxyl glycerol dibiphytanyl glycerol tetraethers in marine sediments: identification of both core and intact polar lipid forms. *Geochim. Cosmochim. Acta* 89, 102–115. doi:10.1016/j.gca.2012.04.053

Liu, X.-L., Summons, R. E., and Hinrichs, K.-U. (2012b). Extending the known range of glycerol ether lipids in the environment: structural assignments based on tandem mass spectral fragmentation patterns. *Rapid Comm. Mass Spectrom.* 26, 2295–2302. doi:10.1002/rcm.6355

Locarnini, R. A., Mishonov, A. V., Baranova, O. K., Boyer, T. P., Zweng, M. M., Garcia, H. E., et al. (2018). in *World Ocean Atlas 2018, volume 1: temperature.* Editor A. Mishonov Technical (NOAA Atlas NESDIS), 81, 52.

Lü, X., Chen, J., Han, T., Yang, H., Wu, W., Ding, W., et al. (2019). Origin of hydroxyl GDGTs and regular isoprenoid GDGTs in suspended particulate matter of Yangtze River Estuary. *Org. Geochem.* 128, 78–85. doi:10.1016/j.orggeochem.2018.12.010

Lü, X., Liu, X.-L., Elling, F. J., Yang, H., Xie, S., Song, J., et al. (2015). Hydroxylated isoprenoid GDGTs in Chinese coastal seas and their potential as a paleotemperature proxy for mid-to-low latitude marginal seas. *Org. Geochem.* 89–90, 31–43. doi:10.1016/j.orggeochem.2015.10.004

Moossen, H., Bendle, J., Seki, O., Quillmann, U., and Kawamura, K. (2015). North Atlantic Holocene climate evolution recorded by high-resolution terrestrial and marine biomarker records. *Quat. Sci. Rev.* 129, 111–127. doi:10.1016/j.quascirev.2015.10.013

Moros, M., Andrews, J. T., Eberl, D. D., and Jansen, E. (2006). Holocene history of drift ice in the northern North Atlantic: evidence for different spatial and temporal modes. *Paleoceanography* 21, 1–10. doi:10.1029/2005pa001214

Moros, M., Emeis, K., Risebrobakken, B., Snowball, I., Kuijpers, A., McManus, J., et al. (2004). Sea surface temperatures and ice rafting in the Holocene North Atlantic: climate influences on northern Europe and Greenland. *Quat. Sci. Rev.* 23, 2113–2126. doi:10.1016/j.quascirev.2004.08.003

Müller, J., Werner, K., Stein, R., Fahl, K., Moros, M., and Jansen, E. (2012). Holocene cooling culminates in sea ice oscillations in Fram Strait. *Quat. Sci. Rev.* 47, 1–14. doi:10.1016/j.quascirev.2012.04.024

Newell, S. E., Fawcett, S. E., and Ward, B. B. (2013). Depth distribution of ammonia oxidation rates and ammonia-oxidizer community composition in the Sargasso Sea. *Limnol. Oceanogr.* 58, 1491–1500. doi:10.4319/lo.2013.58.4.1491

Ólafsdóttir, S., Jennings, A. E., Geirsdóttir, Á., Andrews, J., and Miller, G. H. (2010). Holocene variability of the North Atlantic Irminger current on the south- and northwest shelf of Iceland. *Mar. Micropaleontol.* 77, 101–118. doi:10.1016/j.marmicro.2010.08.002

Painter, S. C. (2011). On the significance of nitrification within the euphotic zone of the subpolar North Atlantic (Iceland basin) during summer 2007. *J. Mar. Sci.* 88, 332–335. doi:10.1016/j.jmarsys.2011.05.001

Park, E., Hefter, J., Fischer, G., Iversen, M. H., Ramondenc, S., Nöthig, E.-M., et al. (2019). Seasonality of archaeal lipid flux and GDGT-based thermometry in sinking particles of high-latitude oceans: Fram Strait (79° N) and Antarctic Polar Front (50° S). *Biogeosciences* 16, 2247–2268. doi:10.5194/bg-16-2247-2019

Pitcher, A., Hopmans, E. C., Mosier, A. C., Park, S. J., Rhee, S. K., Francis, C. A., et al. (2011). Core and intact polar glycerol Dibiphytanyl glycerol tetraether lipids of ammonia-oxidizing archaea enriched from marine and estuarine sediments. *Appl. Environ. Microb.* 77, 3468–3477. doi:10.1128/aem.02758-10

Qin, W., Carlson, L. T., Armbrust, E. V., Devol, A. H., Moffett, J. W., Stahl, D. A., et al. (2015). Confounding effects of oxygen and temperature on the TEX86 signature of marine Thaumarchaeota. *Proc. Natl. Acad. Sci.* 112, 10979–10984. doi:10.1073/pnas.1501568112

R Core Team (2022). *R: a language and environment for statistical computing.* (Vienne, Austria: R Foundation for Statistical Computing). Available at: http://www.R-project.org/.

Rinke, C., Chuvochina, M., Mussig, A. J., Chaumeil, P.-A., Davín, A. A., Waite, D. W., et al. (2021). A standardized archaeal taxonomy for the Genome Taxonomy Database. *Nat. Microbiol.* 6, 946–959. doi:10.1038/s41564-021-00918-8

Rodrigo-Gamiz, M., Rampen, S. W., de Haas, H., Baas, M., Schouten, S., and Sinninghe-Damste, J. S. (2015). Constraints on the applicability of the organic temperature proxies $U^{K'}_{37}$, TEX$_{86}$ and LDI in the subpolar region around Iceland. *Biogeosciences* 12, 6573–6590. doi:10.5194/bg-12-6573-2015

Schlitzer, R. (2021). Ocean data view. Available at: https://odv.awi.de/.

Schouten, S., Hopmans, E. C., Schefuss, E., and Sinninghe Damsté, J. S. (2002). Distributional variations in marine crenarchaeotal membrane lipids: a new tool for reconstructing ancient sea water temperatures? *Earth Planet. Sci. Lett.* 204, 265–274. doi:10.1016/s0012-821x(02)00979-2

Schouten, S., Hopmans, E. C., and Sinninghe Damsté, J. S. (2013). The organic geochemistry of glycerol dialkyl glycerol tetraether lipids: a review. *Org. Geochem.* 54, 19–61. doi:10.1016/j.orggeochem.2012.09.006

Shevenell, A. E., Ingalls, A. E., Domack, E. W., and Kelly, C. (2011). Holocene Southern Ocean sur-face temperature variability west of the Antarctic Peninsula. *Nature* 470, 250–254. doi:10.1038/nature09751

Sinninghe Damsté, J. S., Schouten, S., Hopmans, E. C., van Duin, A. C. T., and Geenevasen, J. A. J. (2002). Crenarchaeol: the characteristic core glycerol dibiphytanyl glycerol tetraether membrane lipid of cosmopolitan pelagic Crenarchaeota. *J. Lipid Res.* 43, 1641–1651. doi:10.1194/jlr.m200148-jlr200

Sinninghe Damsté, J. S., Warden, L. A., Berg, C., Jürgens, K., and Moros, M. (2022). Evaluation of the distributions of hydroxylated glycerol dibiphytanyl glycerol tetraethers (GDGTs) in Holocene Baltic Sea sediments for reconstruction of sea surface temperature: the effect of changing salinity. *Clim. Past.* 18, 2271–2288. doi:10.5194/cp-18-2271-2022

Smith, J. M., Chavez, F. P., and Francis, C. A. (2014). Ammonium uptake by phytoplankton regulates nitrification in the sunlit ocean. *PLoS ONE* 9, e108173. doi:10.1371/journal.pone.0108173

Stefánsson, U. (1962) North Icelandic waters, in *Rit Fiskideildar III. Bind*, 3.

Stefánsson, U. (1968). Dissolved nutrients, oxygen and water masses in the Northern Irminger Sea. *Deep. Sea Res.* 15, 541–575. doi:10.1016/0011-7471(68)90063-6

Stefánsson, U., and Ólafsson, J. (1991). Nutrients and fertility of Icelandic waters. *Rit Fiskid.* 1–56.

Stoner, J. S., Jennings, A., Kristjánsdóttir, G. B., Dunhill, G., Andrews, J. T., and Hardardóttir, J. (2007). A paleomagnetic approach to-ward refining Holocene radiocarbon-based chronologies: paleoceanographic records from the north Iceland (MD99-2269) and east Greenland (MD99-2322) margins. *Paleoceanography* 22, 1–23. doi:10.1029/2006pa001285

Thórdardóttir, T. (1984) Primary production north of Iceland in relation to water masses in May–June 1970–1989, 20. ICES CM, 17.

Tierney, J. E., and Tingley, M. P. (2014). A Bayesian, spatially-varying calibration model for the TEX$_{86}$ proxy. *Geochim. Cosmochim. Acta* 127, 83–106. doi:10.1016/j.gca.2013.11.026

Varma, D., Hopmans, E. C., van Kemenade, Z. R., Kusch, S., Berg, S., Bale, N. J., et al. (2024a). Evaluating isoprenoid hydroxylated GDGT-based temperature proxies in surface sediments from the global ocean. *Geochim. Cosmochim. Acta* 370, 113–127. doi:10.1016/j.gca.2023.12.019

Varma, D., van der Meer, M. T. J., Reichart, G.-J., and Schouten, S. (2024b). Impact of water depth on the distributions and proxies of isoprenoid hydroxylated GDGTs in the Mediterranean Sea and the Red Sea. *Org. Geochem.* 194, 104780. in press. doi:10.1016/j.orggeochem.2024.104780

Villanueva, L., and Coolen, M. J. L. (2022). Contributions of genomics to lipid biomarker research: from paleoclimatology to evolution. *Elements* 18, 87–92. doi:10.2138/gselements.18.2.87

Villanueva, L., Schouten, S., and Sinninghe, D. J. S. (2014). Depth-related distribution of a key gene of the tetraether lipid biosynthetic pathway in marine Thaumarchaeota. *Environ. Microbiol.* 10, 3527–3539. doi:10.1111/1462-2920.12508

Wang, K. J., Huang, Y., Majaneva, M., Belt, S. T., Liao, S., Novak, J., et al. (2021). Group 2i Isochrysidales produce characteristic alkenones reflecting sea ice distribution. *Nat. Comm.* 12, 15–10. doi:10.1038/s41467-020-20187-z

Wei, B., Jia, G., Hefter, J., Kang, M., Park, E., Mollenhauer, G., et al. (2020). Comparison of the $U_{37}^{K'}$, LDI, TEX$_{86}^{H}$ and RI-OH temperature proxies in the northern shelf of the South China Sea. *Biogeosciences* 17, 4489–4508. doi:10.5194/bg-17-4489-2020

Wittenborn, A. K., Bauersachs, T., Hassenrück, C., Käding, K., Wäge-Recchioni, J., Jürgens, K., et al. (2023). *Nitrosopumilus* as main source of isoprenoid glycerol dialkyl glycerol tetraether lipids in the central Baltic Sea. *Front. Microbiol.* 14, 1216130. doi:10.3389/fmicb.2023.1216130

Wuchter, C., Schouten, S., Coolen, M. J. L., and Sinninghe Damsté, J. S. (2004). Temperature-dependent variation in the distribution of tetraether membrane lipids of marine Crenarchaeota: implications for TEX$_{86}$ paleothermometry. *Paleoceanography* 19, PA4028. doi:10.1029/2004pa001041

Xiao, W., Xu, Y., Zhang, C., Lin, J., Wu, W., Lü, X., et al. (2023). Disentangling effects of sea surface temperature and water depth on hydroxylated isoprenoid GDGTs: insights from the hadal zone and global sediments. *Geophys. Res. Lett.* 50, e2023GL103109. doi:10.1029/2023gl103109

Zhang, Y. G., Pagani, M., and Wang, Z. (2016). Ring Index: a new strategy to evaluate the integrity of TEX86 paleothermometry. *Paleoceanogr. Paleoclimatol.* 31, 220–232. doi:10.1002/2015pa002848

Zhu, C., Wakeham, S. G., Elling, F. J., Basse, A., Mollenhauer, G., Versteegh, G. J. M., et al. (2016). Stratification of archaeal membrane lipids in the ocean and implications for adaptation and chemotaxonomy of planktonic archaea. *Environ. Microbiol.* 18, 4324–4336. doi:10.1111/1462-2920.13289

Zweng, M. M., Reagan, J. R., Seidov, D., Boyer, T. P., Locarnini, R. A., Garcia, H. E., et al. (2018). *World Ocean Atlas 2018, volume 2: salinity*. Editor A. Mishonov Technical (NOAA Atlas NESDIS), 82, 50.